Finite element modelling of multielectrode capacitive systems for flow imaging

S.H. Khan
F. Abdullah

Indexing terms: Electrical capacitive tomography, Finite element modelling, CAD of instruments, Flow imaging, Field simulation

Abstract: The CAD of a complex multielectrode arrangement for flow imaging is explored using the finite element method (FEM). This electrode arrangement forms the primary sensor subsystem for an electrical capacitive tomography (ECT) system. Results are presented in the form of sensor's performance parameters as functions of its various geometric parameters. The performance parameters include the standing and normalised capacitances, ratio of the maximum to minimum capacitance of the sensor (Kc) and the sensor's spatial sensitivity distributions. Extensive computer simulation studies were undertaken in calculating these parameters, and the techniques in finite element (FE) model definition, mesh generation and refinement, error minimisation and checking are highlighted in the paper in relation to the effective and efficient use of the FEM. Detailed results for a particular sensor design are compared with an experimental prototype and found to give good agreement. The response of the sensor to various flow regimes is also presented and analysed to optimise its performance for image reconstruction.

1 Introduction

In recent years electrical capacitive technique for measurement and imaging of two-phase flows in real time has gained considerable momentum [1, 2]. The technique involves a number of capacitive electrodes mounted circumferentially around a flow pipe, and relies on changes in capacitance values between electrodes owing to the change in permittivities of flow components. Capacitances are measured between various electrode pairs and the data thus obtained are used to reconstruct cross sectional distribution of flow components. Beck *et al.* [3] first proposed this technique which has been found to have considerable potential for use in process industry, especially oil industry. Compared to other existing tomography systems, electrical capacitive systems are cheap, fast, noninvasive and simple in construction. From now on by 'system' we will mean the primary sensor subsystem of the ECT system.

Fig. 1 shows the cross section of a 12-electrode capacitive system which consists of 12 symmetrically mounted capacitive electrodes on the insulating section of a pipeline. The earthed radial screens in-between the electrodes reduce large capacitances between adjacent electrodes.

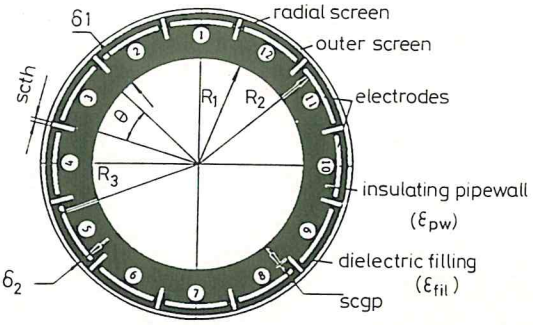

Fig. 1 *Cross section of a 12-electrode capacitive system for ECT flow imaging (not in scale)*

The outer screen with radius R_3 is earthed to shield the electrode system from stray fields. The empty space between this screen and the pipe wall outer surface is filled with dielectric material ($\varepsilon = \varepsilon_{fil}$) which insulates the electrodes from the screen. The thickness of the pipe wall ($\varepsilon = \varepsilon_{pw}$) $\delta_1 = R_2 - R_1$ can be varied by varying the outer radius R_2 while the inner radius R_1 remains constant for a given pipeline.

For data acquisition, one of the electrodes ('active electrode') is given a constant potential and the capacitances between this and other electrodes ('detecting electrodes', kept at zero potential) are measured by discharging the active electrode and measuring the discharging currents (proportional to the unknown capacitances) from the detecting electrodes [1]. For any given pair of electrodes, a region of positive sensitivity can be found inside the pipe within which a unit dielectric increase leads to an increase in their measured capacitances. For all different combinations of electrode pairs, these narrow regions of positive sensitivity create the total positive sensing area of the electrode system over the pipeline cross section. A suitable image reconstruction algorithm could be used to

First of all the authors wish to thank SERC for financing this work under an SERC grant. The authors would also like to thank Prof. M.S. Beck and Dr. C.G. Xie at UMIST for their close collaboration and readiness to help and Dr. S.M. Huang from Schlumberger Cambridge Research Limited, UK for many useful discussions and for providing us with experimental data.

exploit the functional relationship between the measured capacitances, dielectric and sensitivity distribution functions, and solve the inverse problem of determining the flow component distribution over the pipe cross section [2].

The quality of the reconstructed image and the performance of multielectrode capacitive systems depend on the uniformity of sensitivity distribution between electrodes which, in turn, depends on the inherently nonuniform electric field distribution inside the flow pipe. This nonuniformity depends strongly on the geometric and material parameters of the system (θ, δ_1, δ_2, *scgp*, *scth*, the number of electrodes N, ε_{pw} and ε_{fil}) shown in Fig. 1. This necessitates the need for the CAD of electrode systems [4] to optimise their geometric parameters and achieve the best system performance (the material parameters, ε_{pw} and ε_{fil} of an electrode system are often fixed). Basically, this involves the solution of two mutually integrated problems: (i) the forward problem of field analysis and (ii) the inverse problem of image reconstruction. The data obtained from the solution of the forward problem are fed into the image reconstruction algorithm in the form of capacitance measurements and the corresponding sensitivity distribution maps over the flow pipe cross section. Thus it becomes obvious that accurate and reliable field modelling is vitally important for the CAD and performance evaluation of ECT electrode systems. The modelling techniques and strategy adopted in the paper are directly applicable to the CAD of other electrical tomography systems, such as the electrical impedance tomography (EMT) and electromagnetic tomography (EMT). This is because, although these three techniques represent different physical phenomena, mathematically their basic underlying principles are defined by the same set of equations.

2 Finite element modelling of capacitive electrode systems

2.1 Assumptions and the field equation

Two-dimensional (2D) FE modelling of capacitive electrode systems was carried out under the following assumptions: (i) The fringing field effects due to the finite length of electrodes are negligible; this assumes that the electric field distribution remains the same for any plane perpendicular to the axial direction of the flow pipe. (ii) Flow component distribution of a two-component flow does not change spatially along the pipe axial direction (at least not within the electrode length). (iii) Permittivities of flow components remain constant and do not depend on the field; this assumes the linearity of permittivities for any given field.

Under these assumptions, the electric field in the electrode system shown in Fig. 1 is governed by the following Laplace's equation

$$\nabla \cdot [\varepsilon(x, y)\nabla\Phi(x, y)] = 0 \tag{1}$$

This equation is solved by FEM [5] in terms of electrostatic potential $\Phi = \Phi(x, y)$ for given space-varying permittivities of flow component distribution $\varepsilon = \varepsilon(x, y)$. Fig. 2 shows the finite element model of the electrode system shown in Fig. 1 and the boundary conditions under which eqn. 1 is solved. After solving eqn. 1, field intensity and flux density vectors $\boldsymbol{E}$ and $\boldsymbol{D} = \varepsilon\boldsymbol{E}$, and, subsequently, capacitance between any pair of electrodes are calculated from the known potential distributions in the system (see Section 2.2).

2.2 Different aspects of FE modelling

Considering the sensor's geometric features, modelling accuracy requirements and various modelling options the

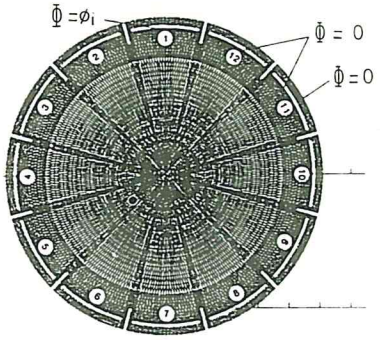

Fig. 2 *Finite element model of 12-electrode capacitive system (full model)*

following aspects have been taken into account: (i) preprocessing time and effort required to set up the model; (ii) symmetry of FE mesh for symmetrically positioned electrodes; (iii) discretisation of the model with finite elements, and its consistency for various sensor models with different geometric parameters; (iv) postprocessing: capacitance calculation; (v) errors.

CAD and FE modelling of capacitive electrode systems could be very computationally intensive, especially when evaluating the performance of systems of different geometric parameters, optimising these parameters and evaluating system response to various flow regimes. It is therefore often desirable to adopt some suitable procedures, with which one can set up adequate system models for given geometric and material parameters and generate a finite element mesh easily and efficiently.

For empty pipe and radially symmetrical flows (e.g. core flow, annular flow), electric field distribution inside the flow pipe is symmetrical along the central line passing through a given active electrode and the electrode positioned diametrically opposite to it (Fig. 3). As a consequence, the capacitances between the active electrode and

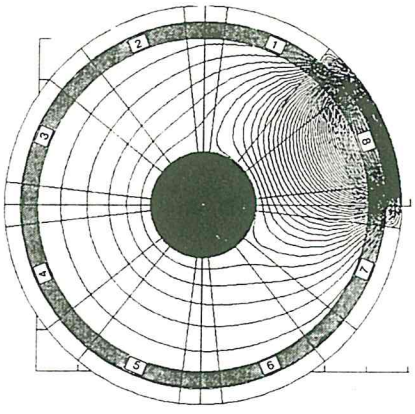

Fig. 3 *Equipotential lines in 8-electrode capacitive system showing symmetry in their distribution*

the electrodes situated symmetrically opposite relative to this line are equal. For example, if electrode 1 (in Fig. 3) is selected as the active electrode, the capacitances between electrode pairs 1–2 and 1–8, 1–3 and 1–7, etc. are equal. To ensure this, the FE mesh of the electrode system must be made symmetrical for symmetrically positioned electrodes (Fig. 2). Furthermore, for the above flow regimes, the symmetry in electric field distribution could be exploited by considering only half of the electrode system with appropriate boundary conditions (Fig. 4) for modelling purposes. This reduces time needed for

model definition and mesh generation, and increases the accuracy of the FE solution as finer mesh can be generated for the same number of nodes.

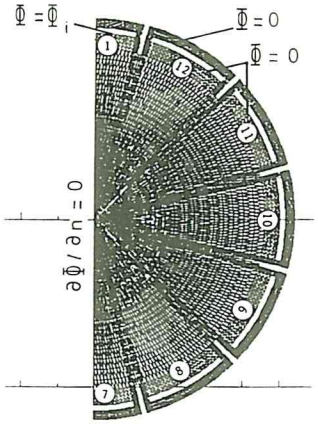

Fig. 4 *Finite element model of 12-electrode capacitive system with boundary conditions (half model)*

In FE analysis, discretisation of the problem area into finite elements plays a key role in the satisfactory completion of model definition in terms of the accuracy of the end results. This is particularly applicable to multi-electrode capacitive systems which, from the FE modelling point of view, mostly consist of annular and curvilinear quadrilateral regions often with sharp corners. As in most cases of FE modelling, finer and better aspect ratio triangles should be used for those regions where rapid changes in potential or field lines are most likely to occur. To ensure comparability of simulation results for a wide range of electrode systems of different geometric parameters, a consistent mesh pattern should be maintained.

Most of the postprocessing associated with capacitive electrode modelling involve capacitance calculations between electrode pairs from field computation results. The capacitance C can be calculated from the total charge Q distributed on the detecting electrode using $C = Q/V$, where V is the potential difference between given electrodes. The charge Q can be obtained from Gauss's law [6] expressed as

$$Q = \oint_s Dn\, ds = \oint_s D \cos\theta\, ds = \oint_s \boldsymbol{D} \cdot \boldsymbol{n}\, ds = \oint_s \boldsymbol{D} \cdot \boldsymbol{ds} \quad (2)$$

Eqn. 2 indicates that the integral of the normal component, $Dn = D\cos\theta = \boldsymbol{D} \cdot \boldsymbol{n}$ of flux density vector $\boldsymbol{D}$ over any closed surface s enclosing the detecting electrode is equal to the total charge Q distributed on it. If the detecting electrode surface, or a surface very close to it, is selected as the integration surface s, the calculation of Q becomes much easier to perform, as there is no need to find Dn since electric field lines are always normal to a conducting surface (e.g. the surface of the detecting electrode). In this case $Q = \oint_s D\, ds$, which gives $C = (\oint_s D\, ds)/V$, where D is the magnitude of $\boldsymbol{D}$.

The main sources of errors in FE modelling of capacitive electrode systems are the discretisation errors and errors in capacitance calculations. Discretisation errors are inherent to the FEM itself and in most cases can only be minimised but never totally eliminated. These errors which mainly depend on the sizes and the shapes of discrete elements can be minimised, for given geometric configurations of various models by using, where possible finer mesh with better aspect ratio triangular elements. To ensure comparability of simulation results from various models, any discretisation error which cannot be reduced by further mesh refinement and other manipulations should be maintained consistent for these models.

As capacitances are calculated from field computation results, the associated errors are, first of all, dependent upon the accuracy of field solutions. Apart from this, the method used for numerical integration in eqn. 2 also contributes to the errors in capacitance calculations.

3 Realisation of finite element models

3.1 Basic model definition

Although the geometry of the electrode system shown in Fig. 1 looks simple, it could be, in fact quite complicated and time consuming to set up the corresponding FE models. For efficient FE model definition, a systematic approach is adopted at the preprocessing stage which exploits the symmetrical geometry of the electrode system. In this, all FE models of the electrode system (like the one shown in Fig. 2) are built from the basic 'building block' shown in Fig. 5. It constitutes only

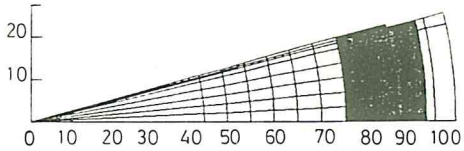

Fig. 5 *Basic 'building block' used to create FE models of 12-electrode capacitive system*

1/24th of the whole model and consists mainly of curvilinear FE regions defined by the model definition commands in the PE2D (the electromagnetic software package used for FE modelling described in this paper) [7]. By successive rotations and mirror reflections of this elementary block, a half (Fig. 4) or a full (Fig. 2) model is created using PE2D's 'copy' command options. All these and other commands are stored in a file ('command input' file) which can be easily updated, modified and called upon at any time to have the commands automatically executed to set up FE models with various geometric parameters.

3.2 FE models for flow response evaluation

FE models of the electrode system could be used to evaluate system response to typical two-phase flow regimes likely to be encountered in practice. These are core, annular and stratified flows as shown schematically in Fig. 6. Flow concentration β (expressed in %) is given

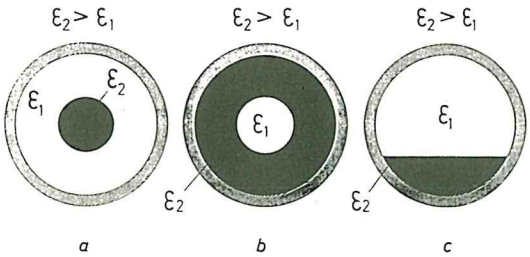

Fig. 6 *Various types of two-phase flow patterns likely to be encountered in practice*

a core flow
b annular flow
c stratified flow

by the ratio of the cross-sectional area of the higher permittivity component, S_2 and that of the flow pipe, S_1; namely $\beta = (S_2/S_1)100\%$, where $S_1 = \pi R_1^2$. By adding

appropriate FE regions in the basic model defined above, models for the simulation of these flow regimes are created. Fig. 7 shows the FE model for core flow simulations which could be used for any given flow concentration. This model could also be used to annular flow

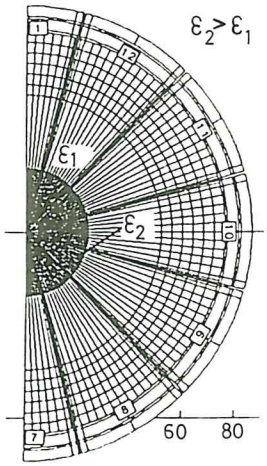

Fig. 7 *FE model for simulation of flow regimes*
10% core flow

regimes simply by interchanging permittivity values of appropriate FE regions. As core and annular flows have radially symmetrical flow component distributions, only a half model of the electrode system needs to be considered. Full FE models for stratified flow simulations could be obtained by adding FE regions inside the pipeline in the basic model. It should be noted that, for all these models, appropriate readjustments of FE region parameters have to be made for different flow concentrations β to ensure a consistent discretisation pattern.

3.3 FE models for experimental electrode systems

FE modelling of two different electrode systems which were used at UMIST for experimental studies have been carried out. By comparing experimental results with simulation data, the FE modelling approach can be validated [8]. Fig. 8 shows the cross section of one of the

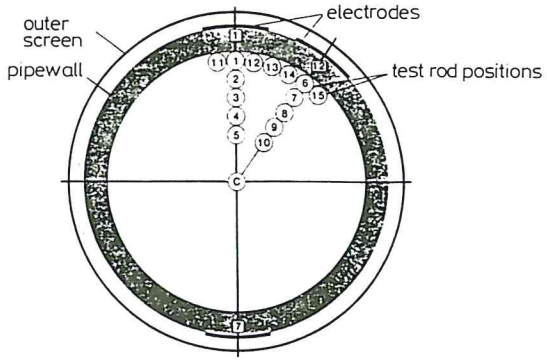

Fig. 8 *Cross section of experimental electrode system showing various test rod positions*
(only three electrodes are shown)

experimental electrode systems without interelectrode radial screens. In the course of experimental studies, capacitances were measured between various electrode pairs and sensitivities of electrode systems were tested by inserting axially a perspex rod of circular cross section at various positions inside the pipeline shown by the encircled numbers in Fig. 8. Fig. 9 shows the FE model of one of the experimental electrode systems (with radial screens) built form the basic 'building block' shown in Fig. 10 (different from the one discussed in Section 3.1 owing to the presence of circular regions for rod positions). Circular regions, representing test rods in Figs. 9 and 10 are made by replicating appropriate annular

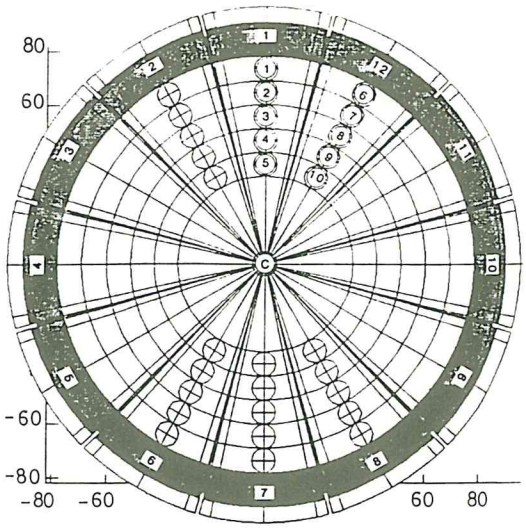

Fig. 9 *Finite element model of thick pipe wall experimental electrode system with radial screens*

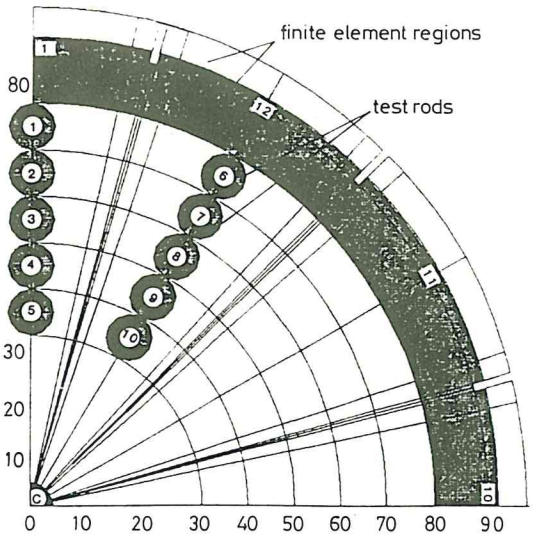

Fig. 10 *Basic 'building block' for FE model definition of experimental electrode system*

regions in local coordinate systems. Permittivities of these regions could be easily changed which allows the modelling of the electrode system with empty pipe as well as with the simulated test rod inserted at one of the rod positions.

3.4 Solution of the field equation and modelling errors

After model definition and FE discretisation, eqn. 1 was solved using the aforementioned software package PE2D running under Unix on a standalone Sun Sparcstation 1. The number of linear triangular elements used for various models of the electrode system varied, approximately, from 9700 (about 5100 nodes) to just under 10 000 (about 5300 nodes). It took about 2–3 minutes to solve the equation and another 3–4 minutes to calculate a set of six capacitances between various electrode pairs.

Although comparison of simulation data with experimental results is the ultimate way to evaluate modelling accuracy, there could be several other alternatives. One

of these is to compare field computation results for different mesh configurations in the same model; this would normally indicate the necessity for further global mesh refinement. In the case of capacitive electrode systems, perhaps the most convenient way of assessing the accuracy of the FE solutions is to calculate the assigned potential difference (given as boundary conditions) $\Delta\Phi$ between the active and detecting electrodes from the field computation results using $\Delta\Phi = -\int \boldsymbol{E} \cdot dl$ [9]. Here l is the length of the path between the active and the detecting electrodes.

Although effective, the above two methods do not give much information about the local errors arising from FE discretisations. This, however, can be readily obtained from the package PE2D, which can display both local and global errors in the field derived from potential solutions [7]. The global error gives indicates the quality of the overall discretisation whereas the local errors show where the FE mesh needs local refinement.

4 Some modelling results and discussion

4.1 System performance parameters

The following performance parameters have been used to evaluate system performance and its responses to variations in the geometric parameters and various flow regimes: (i) standing mode capacitance, C_{0ij}: capacitance between electrode pair i–j when the pipe is empty ($\beta = 0$, $\varepsilon_1 = 1$); (ii) relative sensitivity of the system, $S_{ij} = \Delta C_{ij}/C_{0_{ij}} = (C_{ij} - C_{0_{ij}})/C_{0_{ij}}$, where C_{ij} is the capacitance between electrode pair i–j when the flow pipe is not empty ($\beta \neq 0$, $\varepsilon_1 = 1$, $\varepsilon_2 > 1$); (iii) normalised capacitance, $C_{ij}^n = (C_{ij}^\beta - C_{0_{ij}})/(C_{ij}^f - C_{0_{ij}})$, where C_{ij}^β is the capacitance between electrodes i–j for a given flow concentration β (as defined earlier); C_{ij}^f-the capacitance between electrodes i–j when the pipe is full of material of $\varepsilon = \varepsilon_2$ ($\beta = 100\%$); (iv) ratio of the maximum standing mode capacitance (C_{max}) to the minimum one (C_{min}), $K_c = C_{max}/C_{min}$.

Standing mode capacitance $C_{0_{ij}}$ between diametrically opposite electrode pairs is usually the smallest for a given electrode system. Since the sensitivity requirement of a capacitance measuring circuit depends mainly on this smallest value, it is quite important to be able to predict this by simulations. Relative sensitivity S_{ij} is the measure of the capacitance changes between various electrodes owing to the presence of a small permittivity material inside the flow pipe. Normalised capacitances C_{ij}^n indicate a change of capacitances between those of empty pipe and full pipe for a given flow component distribution. To avoid saturation of sensor electronics owing to large capacitance changes and to ensure satisfactory image reconstruction, it is desirable to limit the values of normalised capacitances so that $0 \leqslant C_{ij}^n \leqslant 1$ [2].

4.2 Validation of FE models

As mentioned earlier in Section 3.3, experimental studies were carried out at UMIST with two different electrode systems. Comparison of simulation results for these systems with the experimental data has validated FE models and therefore established confidence in the CAD technique used for sensor design.

Various standing mode capacitances, obtained by simulations and compared with the corresponding experimental results confirm the effects of radial screens and pipe wall thickness on the system performance parameters. Figs. 11 and 12 show variations in relative sensitivities obtained from both experimental and simulation data for sensor models with and without radial screens. In these Figures, numbers 1 to 10 and 'C' along

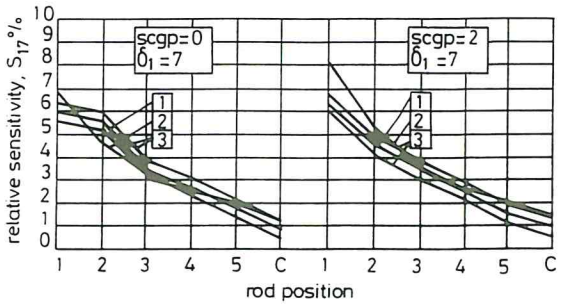

Fig. 11 *Variation of relative sensitivity S_{17} with rod position showing the effects of radial screen depth scgp (δ_1 = constant); 3: experimental error margin; scgp and δ_1 in mm*

Other design parameters: $R_1 = 68$ mm, $\delta_2 = 6$ mm, $\theta = 24°$, $scth = 0$ (electrode system without radial screens $scgp = 0$, $\delta_1 = 7$ mm), $scth = 1.6$ mm (electrode system with radial screens $scgp = 2$ mm, $\delta_1 = 7$ mm), $N = 12$, $\varepsilon_{pw} = 3$, $\varepsilon_{fil} = 1$, radius of test rod $R_{rod} = 4.5$ mm, permittivity of test rod material $\varepsilon_{rod} = 3$
1: experimental; 2: Simulated; 3: error-margin

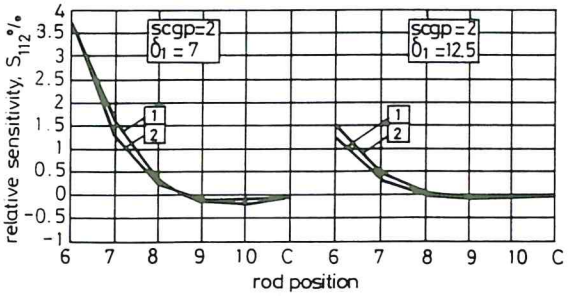

Fig. 12 *Variation of relative sensitivity S_{112} with rod position showing effects of pipe wall thickness δ_1 (scgp = const.); scgp and δ_1 in mm*

Other design parameters: for thin pipe wall electrode system ($\delta_1 = 7$ mm, $scgp = 2$ mm) — $R_1 = 68$ mm, $\delta_2 = 6$ mm, $\theta = 24°$, $scth = 1.6$ mm, $N = 12$, $\varepsilon_{pw} = 3$, $\varepsilon_{fil} = 1$, $R_{rod} = 4.5$ mm, $\varepsilon_{rod} = 3$; for thick-pipe wall electrode system ($\delta_1 = 12.5$ mm, $scgp = 2$ mm) — $R_1 = 78$ mm, $\delta_2 = 6$ mm, $\theta = 25°$, $scth = 1.6$ mm, $N = 12$, $\varepsilon_{pw} = 3$, $\varepsilon_{fil} = 1$, $R_{rod} = 4.5$ mm, $\varepsilon_{rod} = 3$
1: Experimental; 2: Simulated

x-axis represent the test rod positions shown in Fig. 9. Both simulation and experimental results reflect the effects of pipe wall thickness (Fig. 12) and radial screen depth (Fig. 11) on sensitivity distributions inside the pipe. As can be seen from these Figures, the deviations of simulation results from experimental ones vary differently for different electrode pairs and electrode designs. Although simulation results for sensitivities S_{17} show reasonable agreement with the experimental ones, some disagreement could be observed for negative sensitivities S_{112} (Fig. 12). This is particularly true for the test rod at positions 9, 10 and 'C', where very small capacitance changes ΔC_{112} have been obtained. All these differences between simulation and experimental results are attributed to various experimental [1] and modelling errors which could be minimised. Further details on the above simulation results can be found in Reference 8.

4.3 Effects of variations of system geometric parameters

The effects of various geometric parameters of the electrode system (Fig. 1) on system performance have been investigated by FE modelling and analysed in Reference 4. In this Section, some of the most interesting results are presented.

For a given sensor design, electrode angle θ is related to the number of electrodes N. Provided that the

electrode–electrode angular distance remains constant, θ always decreases with the increase of N. This deteriorates the system performance by reducing the standing mode capacitances C_{0ij} and therefore increasing the minimum detectable void fraction.

It is obvious from the geometry of the electrode system (Fig. 1) that the capacitances between adjacent electrodes (e.g. C_{0112} between 1 and 12) are usually the largest and those between diametrically opposite ones (e.g. C_{017}) the smallest. These are referred to as C_{max} and C_{min}, respectively. Increased measurement accuracy can be obtained by minimising their ratio K_c, the value of which, for example, depends on θ (Fig. 13) and the outer screen distance from the pipe wall δ_2 (Fig. 14). These Figures also

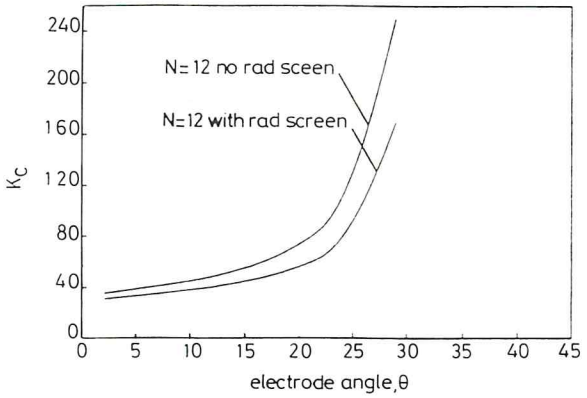

Fig. 13 *Effects of electrode angle θ and radial screens on K_c*

Other design parameters: $R_1 = 38$ mm, $\delta_1 = 5$ mm, $\delta_2 = 4$ mm, $scth = 0$ (electrode system without radial screens), $scth = 0.1$ mm (electrode system with radial screens), $scgp = 0$, $N = 12$, $\varepsilon_{pw} = 3$, $\varepsilon_{fil} = 1$

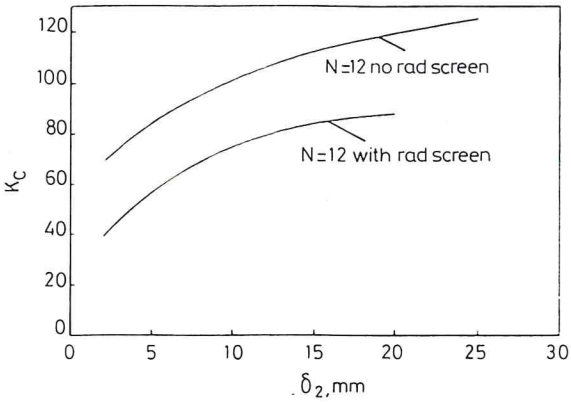

Fig. 14 *Variation of K_c with outer screen distance from pipe wall δ_2*

Other design parameters: $R_1 = 38$ mm, $\delta_1 = 5$ mm, $\theta = 22°$, $scgp = 0$, $scth = 0$ (electrode system without radial screens), $scth = 0.1$ mm (electrode system with radial screens), $N = 12$, $\varepsilon_{pw} = 3$, $\varepsilon_{fil} = 1$

show the positive effects of radial screens in reducing the capacitances between adjacent electrodes by shielding electric fields from the active electrode. Qualitatively, this is evident from the equipotential plots in the vicinity of the active (electrode 1) and the adjacent (electrode 12) electrodes for two different electrode designs: without (Fig. 15*a*) and with (Fig. 15*b*) radial screens. The effectiveness of radial screens in reducing capacitances (and hence K_c), especially between adjacent electrodes, depends on the combination of their geometric parameters *scgp* and screen thickness *scth* (Fig. 16) and pipe wall thickness δ_1 (Fig. 17). Moreover, as already shown in the previous Section, the selection of *scgp* and δ_1 plays a key role in determining the uniformity of sensitivity distributions inside the flow pipe and therefore to a great extent affects the quality of the reconstructed images. It will be shown in the following Section that *scgp* and δ_1 affect the range of normalised capacitances C_{ij}^n which also determines the quality of the reconstructed images.

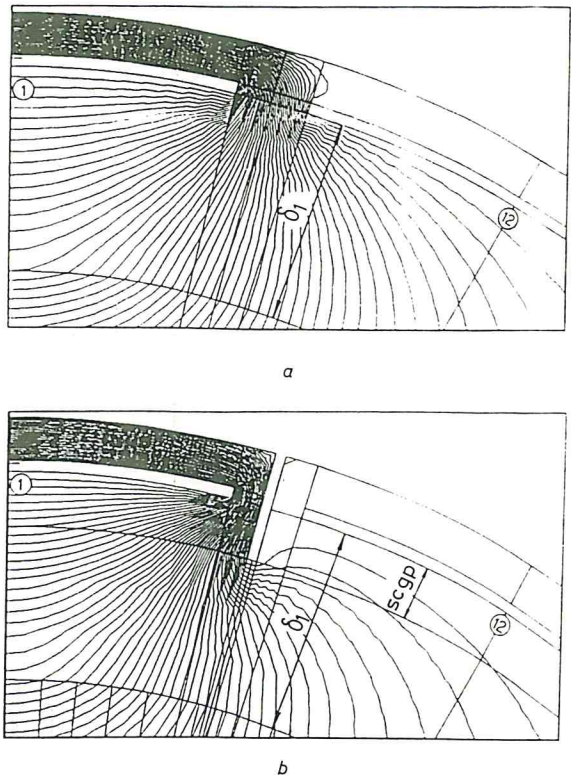

Fig. 15 *Equipotential contours for 12-electrode capacitive systems showing effects of radial screens*

a without
b with radial screens

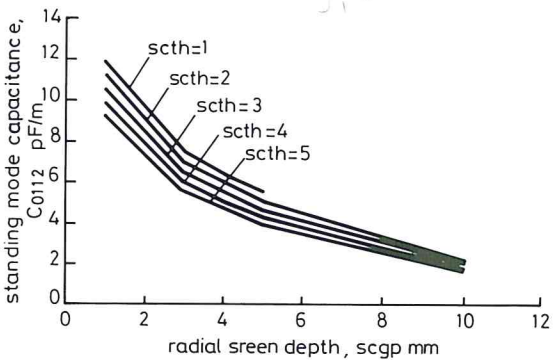

Fig. 16 *Variation of standing mode capacitance C_{0112} with radial screen depth scgp (δ_1 = const.); radial screen thickness scth in mm*

Other design parameters: $R_1 = 76.2$ mm, $\delta_1 = 19.05$ mm, $\delta_2 = 5$ mm, $\theta = 25.8°$, $N = 12$, $\varepsilon_{pw} = 3$, $\varepsilon_{fil} = 1$

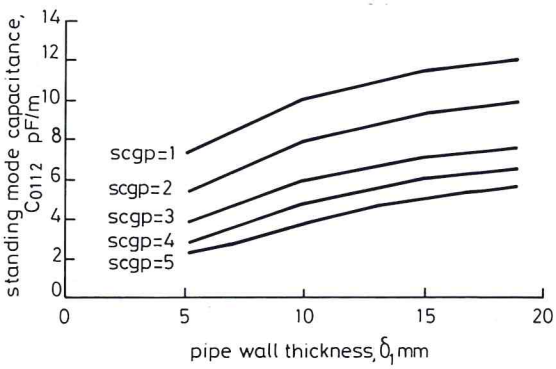

Fig. 17 *Variation of standing mode capacitance C_{0112} with pipe wall thickness δ_1 (scth = const.); radial screen depth scgp in mm*

Other design parameters: $R_1 = 76.2$ mm, $\delta_2 = 5$ mm, $\theta = 25.8°$, $scth = 1$ mm, $N = 12$, $\varepsilon_{pw} = 3$, $\varepsilon_{fil} = 1$

4.4 System response to various flows

Simulation of various flow regimes discussed in Section 3.2 is essential to the evaluation of system response to these flows in terms of normalised capacitances C_{ij}^n. FE modelling of the electrode system allows one to vary, and see, the effects of such key geometric parameters as δ_1 and *scgp* on normalised capacitances for various flow regimes. Fig. 18 shows some of the modelling results for

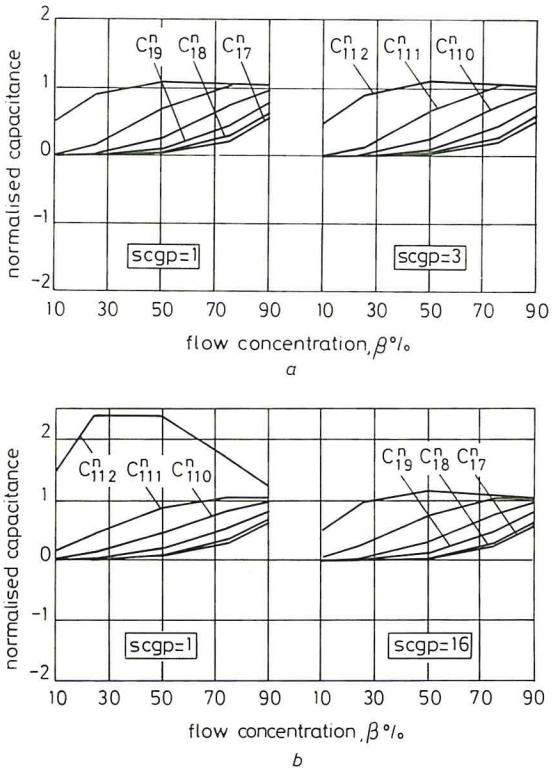

Fig. 18 *Effects of flow concentration β and radial screen depth scgp on normalised capacitances C_{ij}^n (annular flow); scgp in mm*

a $\delta_1 = 5$ mm
b $\delta_1 = 20$ mm
Other design parameters: $R_1 = 76.2$ mm, $\delta_2 = 5$ mm, $\theta = 25.8°$, *scth* = 1 mm, $N = 12$, $\varepsilon_{pw} = 5.9$, $\varepsilon_{fil} = 4$, $\varepsilon_1 = 1$, $\varepsilon_2 = 3$

annular flow regimes of various concentrations β. Two extreme cases of pipe wall thickness δ_1 have been considered: $\delta_1 = 5$ mm (Fig. 18*a*) and $\delta_1 = 20$ mm (Fig. 18*b*). As can be seen from Fig. 18*a*, for thin pipe wall electrode systems, normalised capacitances mostly remain between 0 and 1 and virtually independent of the radial screen penetration depth *scgp*. In the case of the thick pipe wall electrode system, large values of normalised capacitances between adjacent electrodes C_{112}^n (electrode 1 is the active electrode) are observed for smaller *scgp*. These large C_{112}^n can be reduced by adequately increasing the radial screen penetration depth (Fig. 18*b*). These, and other simulation results, suggest that almost identical responses to both core and annular flow regimes can be obtained from thick and thin pipe wall electrode systems, provided that the radial screen depth is chosen correctly.

5 Conclusions

An industrial prototype of a 12-electrode capacitive flow imaging system has been successfully tested at Schlumberger Cambridge Research Limited, UK [10]. The primary sensor system used has been designed and optimised by the FE modelling techniques described in this paper. This establishes the importance and effectiveness of such CAD techniques in ECT sensor design. It has been shown that virtually all aspects of design, performance evaluation and characterisation of these multi-electrode sensor systems could be tackled effectively and efficiently by CAD techniques based on FE modelling.

6 References

1 HUANG, S.M., XIE, C.G., THORN, R., SNOWDEN, D., and BECK, M.S.: 'Design of sensor electronics for electrical capacitance tomography', *IEE Proc. G*, 1992, **139,** (1), pp. 83–88
2 XIE, C.G., HUANG, S.M., HOYLE, B.S., THORN, R., LENN, C., SNOWDEN, D., and BECK M.S.: 'Electrical capacitance tomography for flow imaging: system model for development of image reconstruction algorithms and design of primary sensors', *IEE Proc. G*, 1992, **139,** (1), pp. 89–98
3 BECK, M.S., PLASKOWSKI, A., and GREEN, R.G.: 'Imaging for measurement of two-phase flow', *in* VERET, C. (Ed.): 'Flow visualization IV'. Proceedings of the 4th International Symposium on *Flow Visualization*, 26–28 August 1986 (Hemisphere Publishing Corporation), pp. 585–588
4 KHAN, S.H., and ABDULLAH, F.: 'Computer aided design of process tomography capacitance electrode system for flow imaging', *in* GRATTAN, K.T.V. (Ed.): 'Sensors: Technology, systems and applications' (Adam Hilger, Bristol, 1991), pp. 209–214
5 SILVESTER, P.P., and FERRARI, R.L.: 'Finite elements for electrical engineers' (Cambridge: Cambridge University Press, 1990, 2nd edn)
6 RAMO, S., WHINNERY, J.R., and DUZER, T.V.: 'Fields and waves in communication electronics' (John Wiley & Sons, Inc., New York, 1965)
7 'The PE2D reference manual, version 8.2'. Vector Fields Limited (Oxford: 1990)
8 KHAN, S.H., and ABDULLAH, F.: 'Validation of finite element modelling of multielectrode capacitive system for process tomography flow imaging'. Proceedings of the European Concerted Action on *Process Tomography*, March, 1992, Manchester, pp. 29–39
9 BINNS, K.J., and LAWRENSON, P.J.: 'Analysis and computation of electric and magnetic field problems' (Oxford: Pergamon Press Ltd., 1973, 2nd edn)
10 BECK, M.S., HOYLE, B.S., and LENN, C.P.: 'Process tomography in pipelines', *SERC Bull.*, 1992, **4,** (10), pp. 24–25